MINISTRY OF EDUCATION AND TRAINING
HCMC UNIVERCITY OF TECHNOLOGY AND EDUCATION

DEVELOPMENT OF STOCHASTIC COMPOSITE PLATE MODELS SUBJECTED TO MECHANICAL AND THERMAL LOADS

Major: Engineering mechanics
Specialized code: 9520101

SUMMARY OF DOCTORAL DISSERTATION

HO CHI MINH CITY – 2025

Dissertation is completed at HCMC Univercity of Technology and Education

Supervisor 1:
Supervisor 2:

Reviewer 1:
Reviewer 2:
Reviewer 3:

LIST OF PUBLICATIONS

International Journal Articles

1. Stochastic vibration and buckling analysis of functionally graded microplates with a unified higher-order shear deformation theory, Thin-Walled Structures, vol.177, p.109473,8/ 2022, SCIE (Q1). https://doi.org/10.1016/j.tws.2022.109473

2. Vibration and buckling optimization of porous functionally graded microplates using BCMO-ANN algorithm, Thin-Walled Structures, Thin-Walled Structures, vol. 182, p. 110267, 01/2023, SCIE (Q1). https://doi.org/10.1016/j.tws.2022.110267

3. Stochastic collocation method for thermal buckling and vibration analysis of functionally graded sandwich microplates, Journal of Thermal Stresses, vol. 46, p. 909-934, 6/2023, SCIE (Q2). https://doi.org/10.1080/01495739.2023.2217243

4. An intelligent computational iBCMO-DNN algorithm for stochastic thermal buckling analysis of functionally graded porous microplates using modified strain gradient theory, Journal of Thermal Stresses, online, 7/2024, SCIE (Q2). https://doi.org/10.1080/01495739.2024.2368054

5. Meta-heuristic optimization algorithms for vibration and buckling analysis of laminated composite plates, Engineering Analysis with Boundary Elements, vol.169, Part A, 12/ 2024, 105974, https://doi.org/10.1016/j.enganabound.2024.105974. SCI (Q1).

6. Novel computational algorithms for vibration, buckling, and transient analysis of porous metal foam microplates, Journal of Vibration Engineering & Technologies, 12/2024 accepted.

Domestic journal article

1. Static and vibration analysis of functionally graded microplate with porosities based on higher-order shear deformation and modified strain gradient theory, Vietnam Journal of Mechanics, 2023, ACI. https://doi.org/10.15625/0866-7136/17552

International Conferences

1. A general framework of higher-order shear deformation theory for free vibration analysis of functionally graded microplates, Proceedings of the Second International Conference on Sustainable Civil Engineering and Architecture (ICSCEA-2021), Lecture Notes in Civil Engineering, vol.268, 713–727 2023, index scopus_Q4. https://doi.org/10.1007/978-981-19-3303-5_64

2. An Efficient Size-Dependent Computational Approach for Functionally Graded Porous Sandwich Microplates Based on Modified Couple Stress Theory, International Conference on Green Technology and Sustainable Development (GTSD 2022), Lecture Notes in Networks and Systems, vol 567, 82-96, 2023, index scopus_Q4 https://doi.org/10.1007/978-3-031-19694-2_8

National Conference

1. A BCMO-DNN algorithm for vibration optimization of functionally graded porous microplates, Tuyển tập công trình khoa học Hội nghị Cơ học toàn quốc lần thứ XI (NACOME2 022), Nhà xuất bản Khoa học tự nhiênvà Công nghệ, Tập 1, 577-588, 2022.

CHAPTER 1 INTRODUCTION

Due to their superior hardness and lightness, laminated composite materials are widely utilized in fields like mechanical engineering, aerospace, and construction. However, their layered structure leads to stress concentrations and potential delamination at the interfaces. Thus, functionally graded materials (FGMs) have been developed to address this, offering a continuous variation in material properties along specific directions. Recent advancements have also enabled the production of functionally graded porous materials and porous metal foam materials, which enhance sound dampening and reduce structural weight, making them highly valuable for modern applications. However, the development of such materials accompanied efficiently computational methods and models in order to predict accurately their responses at different structural scales. Therefore, this dissertation carried out the "**development of stochastic composite plate models subjected to mechanical and thermal loads**".

CHAPTER 2 OVERVIEW OF THEORETICAL BASIS

2.1 Advanced composite materials for analysis of plates

2.1.1 Laminated composite materials

Due to their many advantages in stiffness and lightness, laminated composite materials have been widely applied in many engineering fields, such as aviation and construction, mechanical engineering, etc. The LC structure is made of two or more layers of component composite materials that are bonded together at the interface between the layers.

2.1.2 Functionally graded materials

The material properties such as Young's modulus E, mass density ρ, Poisson's ratio ν of FGP material can be approximated by the following expressions .

$$P(x_3) = (P_c - P_m)V_c(x_3) + P_m - 0.5\beta(P_c + P_m) \tag{2.1}$$

2.1.3 Functionally graded sandwich materials

Sandwich structures offer numerous advantages, such as being lightweight and having high bending stiffness, making them ideal for use in aircraft, aerospace, flexible electronics, and biomedical applications. A typical sandwich structure consists of two FGMs face sheets with a homogeneous core in between.

2.1.4 Porous metal foam materials

The effective material properties of porous metal foam materials: Distribution of uniform porosity; Distribution of asymmetric porosity; Distribution of symmetric porosity.

2.2 Plates theories

In the context of plates, the displacement field is expressed in terms of unknown functions ϕ_i^j of the surface coordinates (x_1, x_2) and time t.

$$u_i(x_1, x_2, x_3, t) = \sum_{j=0}^{N} (x_3)^j \phi_i^j(x_1, x_2, t) \tag{2.12}$$

The explicit form of Eq. (2.12) varies depending on the kinematics of the deformation being considered including CPT, FSDT, HSDT, Quasi-3D, and three-dimensional elasticity.

2.3 Size dependent analysis of microplates

The MST proposed by Lam modified the classical strain gradient theory of Mindlin, Mindlin and Eshel to establish a new set of high-order metrics, where the total number of MLSP was reduced from five to three.

$$\delta\Pi_{UB} = \int_A (\boldsymbol{\sigma}\delta\boldsymbol{\varepsilon} + \mathbf{p}\delta\boldsymbol{\xi} + \boldsymbol{\tau}\delta\boldsymbol{\eta} + \mathbf{m}\delta\boldsymbol{\chi})\, dA \tag{2.20}$$

where $\boldsymbol{\varepsilon}, \boldsymbol{\chi}, \boldsymbol{\xi}, \boldsymbol{\eta}$ are strains, symmetric rotation gradients, dilatation gradient and deviation stretch gradient, respectively; $\boldsymbol{\sigma}$ is Cauchy stress; $\mathbf{m}, \mathbf{p}, \boldsymbol{\tau}$ are high-order stresses corresponding with strain gradients $\boldsymbol{\chi}, \boldsymbol{\xi}, \boldsymbol{\eta}$, respectively.

2.4 Ritz solution

The Ritz method was initially introduced by Walter Ritz to analyze the free vibrations of structures.

$$\left\{u_1^0(x_1, x_2, t), \varphi_1(x_1, x_2, t)\right\} = \sum_{j=1}^{N_1}\sum_{i=1}^{N_2} \left\{u_{1ji}(t), x_{ji}(t)\right\} F_{j,1}(x_1) P_i(x_2) \tag{2.24a}$$

$$\left\{u_2^0(x_1, x_2, t), \varphi_2(x_1, x_2, t)\right\} = \sum_{j=1}^{N_1}\sum_{i=1}^{N_2} \left\{u_{2ji}(t), y_{ji}(t)\right\} F_j(x_1) P_{i,2}(x_2) \tag{2.24b}$$

$$u_3^0(x_1, x_2, t) = \sum_{j=1}^{N_1}\sum_{i=1}^{N_2} u_{3ji}(t) F_j(x_1) P_i(x_2) \tag{2.24c}$$

where $u_{1ji}, u_{2ji}, u_{3ji}, x_{ji}, y_{ji}$ are variables that need to be calculated; the shape functions in the x_1- and x_2- directions are represented by $F_j(x_1), P_i(x_2)$.

2.5 Stochastic method

Monte Carlo Simulation (MCS) method is the simplest and most popular approach to solve this complicated problem. Another approach is to use polynomial chaos expansion (PCE) which speeds up the computing process

while still maintains the accuracy. Stochastic collocation (SC) is known as one of stochastic expansion method similar to the popular PCE.

2.6 Neural network systems

Besides, the combination between the BCMO algorithm and ANN to determine optimal responses for FG microplates with uncertainties of material properties has not been developed yet, this interesting topic needs to be investigated. Moreover, a novel intelligent computation algorithm iBCMO-DNN for solving the stochastic thermal buckling problems of FGP microplates by using the MST, unified HSDT and Ritz method will propose.

2.7 Meta-heuristic algorithms

In contrast to optimization algorithms and iterative methods, meta-heuristics algorithms do not ensure the discovery of a globally optimal solution for certain problem classes. Three algorithms including differential evolution (DE), shrimp and goby association search algorithm (SGA) and balancing composite motion optimization (BCMO) are used to solve the above problem.

2.8 Conclusion

A literature review shows that it is necessary to develop stochastic composite plate models subjected to mechanical and thermal loads. For this aim, the dissertation will focus on the contents:

- Develop the new hybrid shape functions for the Ritz method.
- Develop stochastic models to investigate the behaviors of microplates with uncertain material properties.
- Develop new computation algorithms using artificial intelligence to solve the stochastic problems of microplates.
- Propose optimization methods to search the optimal fiber directions of laminated composite plates.

CHAPTER 3: A RITZ-BASED COMPUTATIONAL METHOD FOR SIZE-DEPENDENT ANALYSIS OF ADVANCED COMPOSITE MICROPLATES UNDER THERMO-MECHANICAL LOADS

3.1 Introduction

This chapter proposes various new computational algorithms, which combined the Ritz method under novel shape functions with unified higher- order shear deformation theory and modified strain gradient for analysis of microplates. The characteristic equations are derived using Hamilton's principle and solved by using Ritz solutions.

3.2 Theoretical formulation

3.2.1 Advanced functionally graded materials

3.2.1.1 Porous metal foam material

Consider a rectangular microplate made of porous metal foam (PMF) material. The microplate has a thickness h and sides $a \times b$. Fig. 3.1 displays the material properties of three different types of porosity distributions throughout the thickness of the PMF microplates. The connection between mass density ρ and Young's modulus E can be expressed as follows:

- Distribution of uniform porosity

$$\rho(z) = \rho_{\max}\sqrt{(1-\beta\upsilon)}\;;\; E(z) = E_{\max}(1-\beta\upsilon) \tag{3.1}$$

- Distribution of asymmetric porosity

$$\rho(z) = \rho_{\max}\left[1-\beta_m \cos\left(\frac{\pi z}{2h}+\frac{\pi}{4}\right)\right];\; E(z) = E_{\max}\left[1-\beta\cos\left(\frac{\pi z}{2h}+\frac{\pi}{4}\right)\right] \tag{3.2}$$

- Distribution of symmetric porosity

$$\rho(z) = \rho_{\max}\left(1-\beta_m \cos\left(\frac{\pi z}{h}\right)\right)\;;\; E(z) = E_{\max}\left(1-\beta\cos\left(\frac{\pi z}{h}\right)\right) \tag{3.3}$$

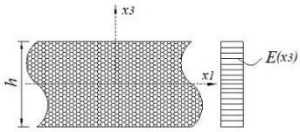

(a) Porosity is uniformly distribution

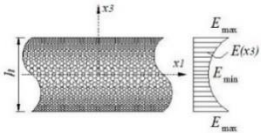

(b)Porosity is symmetric distribution

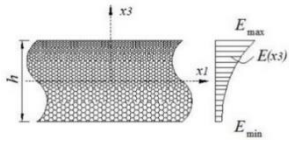

(c) Porosity is asymmetric distribution

Figure 3.1: Three types of porous metal microplates

where $E_{\max}$ and $\rho_{\max}$ are maximum values of Young's modulus and mass density, respectively; β and β_m denotes the porosity parameters and mass density, which are given by:

$$\beta = 1-E_{\min}/E_{\max}, 0<\beta<1\;;\; \beta_m = 1-\frac{\rho_{\min}}{\rho_{\max}}, 0<\beta_m<1 \tag{3.4}$$

where $E_{\min}$ and $\rho_{\min}$ are minimum Young's modulus and mass density.

In which

$$\beta_m = 1-\sqrt{1-\beta} \tag{3.5}$$

The material characteristics in the case of a distribution of uniform porosity remain constant in the thickness direction and depend only on the porosity coefficient β. Thereafter, the coefficient υ is written as follows:

$$\upsilon = 1/\beta - \left(\left(2\sqrt{1-\beta}\right)/\pi - 2/\pi + 1\right)^2/\beta \tag{3.6}$$

3.2.1.2 FG sandwich microplates

The following formulas can be used to evaluate the effective material properties of FG sandwich microplates:

$$P(x_3) = (P_c - P_m)V_c(x_3) + P_m \tag{3.7}$$

where the volume fraction of the ceramic material $V_c(x_3)$ across the plate thickness is determined by Eq (4.3).

with the power-law index p, P_c and P_m are the characteristics of ceramic and metal materials, respectively, such as the Young's moduli E, mass density ρ, and Poisson's ratio ν.

$$V_c(x_3) = \begin{cases} \left(\dfrac{z_4 - x_3}{z_4 - z_3}\right)^p, & z_3 \le x_3 \le z_4 \quad \text{FG top layer} \\ 1 & z_2 \le x_3 \le z_3 \quad \text{ceramic core layer} \\ \left(\dfrac{x_3 - z_1}{z_2 - z_1}\right)^p & z_1 \le x_3 \le z_2 \quad \text{FG bottom layer} \end{cases} \tag{3.8}$$

3.2.1.3 Functionally graded porous materials

The effective material properties of FGP microplates are given by:

$$P(x_3) = (P_c - P_m)\left(\frac{2x_3 + h}{2h}\right)^p + P_m - \frac{\beta}{2}(P_c + P_m) \tag{3.9}$$

where P_c and P_m are the Poisson's ratio ν, Young's moduli E of ceramic and metal materials, respectively; p is the power-law index; $0 \le \beta \ll 1$ is the porosity volume fraction; $x_3 \in [-h/2, h/2]$.

3.2.1.4 Properties of materials and temperature distribution

Moreover, in order to investigate the effect of temperature on the buckling responses, three types of temperature distribution are considered as below:

- For uniform distribution (UTR): $T(z) = T_o + \Delta T$ where the bottom surface's reference temperature is T_o.
- For linear distribution (LTR): $T(z) = (T_t - T_b)(z/h + 0.5) + T_b$ where the temperatures at the top and bottom surfaces of FGP microplates are represented by T_t and T_b, respectively.

- For the nonlinear temperature rise (NLTR): the expression of the current temperature is derived from the Fourier equation of steady-state heat conduction as follows: $T(z)=T(b)+\dfrac{T_t-T_b}{\int_{-h/2}^{h/2}1/k(z)dz}\int_{-h/2}^{z}\dfrac{1}{k(\xi)d\xi}$

where $k(z)$ is the coefficient of thermal conductivity.

3.2.2 Modified strain gradient theory based on a framework of unified high-order shear deformation theory

For simplicity purpose, the effects of transverse normal strain are neglected, i.e. $u_3(x_1,x_2,x_3)=u_3^0(x_1,x_2)$ where $u_3^0(x_1,x_2)$ is transverse displacement at the mid-surface of the microplates. Moreover, it is supposed that the transverse shear stresses are expressed in terms of the transverse shear forces as follows:

$$\sigma_{13}=f_{,3}(x_3)Q_1(x_1,x_2);\ \sigma_{23}=f_{,3}(x_3)Q_2(x_1,x_2) \tag{3.10}$$

where $f(x_3)$ is a higher-order term whose first derivative satisfies the free-stress boundary condition at the top and bottom surfaces of the microplates, i.e. $f_{,3}(x_3=\pm 0.5h)=0$; $Q_1(x_1,x_2),Q_2(x_1,x_2)$ are the transverse shear forces. Additionally, transverse shear strains are linearly related to the membrane displacements $u_1(x_1,x_2,x_3),u_2(x_1,x_2,x_3)$ and transverse one $u_3^0(x_1,x_2)$ by:

$$\gamma_{13}=u_{1,3}+u_{3,1}^0=\frac{\sigma_{13}}{\mu}=\frac{f_{,3}Q_1}{\mu}\ ;\ \gamma_{23}=u_{2,3}+u_{3,2}^0=\frac{\sigma_{23}}{\mu}=\frac{f_{,3}Q_2}{\mu} \tag{3.11}$$

where $\mu(x_3)=E(x_3)/(2(1+\nu))$ is the shear modulus. Furthermore, integrating Eq. (3.11) in x_3-direction leads to a general displacement field of the microplates as follows:

$$u_1(x_1,x_2,x_3)=u_1^0(x_1,x_2)-x_3u_{3,1}^0+\Psi(x_3)Q_1(x_1,x_2) \tag{3.12a}$$

$$u_2(x_1,x_2,x_3)=u_2^0(x_1,x_2)-x_3u_{3,2}^0+\Psi(x_3)Q_2(x_1,x_2) \tag{3.12b}$$

$$u_3(x_1,x_2,x_3)=u_3^0(x_1,x_2) \tag{3.12c}$$

where $\Psi(x_3)=\int_0^{x_3}\dfrac{f_{,3}}{\mu(x_3)}dx_3$. Moreover, it is known that the transverse shear forces can be expressed in terms of the rotation (φ_1,φ_2) and gradients of the transverse displacement as follows:

$$Q_1(x_1,x_2)=H^s(\varphi_1+u_{3,1}^0);\ Q_2(x_1,x_2)=H^s(\varphi_2+u_{3,2}^0) \tag{3.13}$$

where $H^s = k^s \int_{-h/2}^{h/2} \mu(x_3)\, dx_3$ is the transverse shear stiffness of the microplates; $k^s = 5/6$ is shear coefficient factor. Substituting Eq. (3.13) into Eq. (3.12) leads to a general HSDT as follows:

$$u_1(x_1, x_2, x_3) = u_1^0(x_1, x_2) + \Phi_1(x_3) u_{3,1}^0 + \Phi_2(x_3) \varphi_1(x_1, x_2) \tag{3.14a}$$

$$u_2(x_1, x_2, x_3) = u_2^0(x_1, x_2) + \Phi_1(x_3) u_{3,2}^0 + \Phi_2(x_3) \varphi_2(x_1, x_2) \tag{3.14b}$$

$$u_3(x_1, x_2, x_3) = u_3^0(x_1, x_2) \tag{3.14c}$$

where $\Phi_1(x_3) = H^s \Psi(x_3) - x_3, \Phi_2(x_3) = H^s \Psi(x_3)$.

The microplates' total potential energy is calculated by using Hamilton's principle as follows:

$$\int_{t_1}^{t_2} \left(\delta\Pi_{UB} + \delta\Pi_{VB} + \delta\Pi_{FB} - \delta\Pi_{KB} \right) dt = 0 \tag{3.15}$$

where $\delta\Pi_{VB}, \delta\Pi_{UB}$, $\delta\Pi_{FB}$ and $\delta\Pi_{KB}$ are the variations of work done by membrane compressive forces, strain energy, work done by external forces and kinetic energy, respectively. The strain energy variation of the system $\delta\Pi_{UB}$ is obtained by the MST:

$$\delta\Pi_{UB} = \int_A \left(\boldsymbol{\sigma} \delta\boldsymbol{\varepsilon} + \mathbf{p} \delta\boldsymbol{\xi} + \boldsymbol{\tau} \delta\boldsymbol{\eta} + \mathbf{m} \delta\boldsymbol{\chi} \right) dA \tag{3.16}$$

where $\boldsymbol{\varepsilon}, \boldsymbol{\chi}, \boldsymbol{\xi}, \boldsymbol{\eta}$ are strains, symmetric rotation gradients, dilatation gradient and deviation stretch gradient, respectively; $\boldsymbol{\sigma}$ is Cauchy stress; $\mathbf{m}, \mathbf{p}, \boldsymbol{\tau}$ are high-order stresses corresponding with strain gradients $\boldsymbol{\chi}, \boldsymbol{\xi}, \boldsymbol{\eta}$, respectively.

The components of strain ε_{ij} and strain gradients $\xi_i, \eta_{ijk}, \chi_{ij}$ are defined as follows:

$$\begin{aligned} &\varepsilon_{ij} = \left(u_{i,j} + u_{j,i} \right)/2 \; ; \; \xi_i = \varepsilon_{mm,i} \; ; \; \chi_{ij} = \left(u_{n,mj} e_{imn} + u_{n,mi} e_{jmn} \right)/4 \\ &\eta_{ijk} = \left(\varepsilon_{jk,i} + \varepsilon_{ki,j} + \varepsilon_{ij,k} \right)/3 - \left[\left(\xi_i + 2\varepsilon_{mi,m} \right) \delta_{jk} + \left(\xi_k + 2\varepsilon_{mk,m} \right) \delta_{ij} \right. \\ &\left. + \left(\xi_j + 2\varepsilon_{mj,m} \right) \delta_{ki} \right] /15 \end{aligned} \tag{3.17}$$

where δ_{ij} is Knonecker delta; e_{imn} is permutation symbol. The constitutive equations are used to determine the stress components as follows:

$$\sigma_{ij} = \lambda \varepsilon_{kk} \delta_{ij} + 2\mu\varepsilon_{ij} \; ; \; m_{ij} = 2\mu l_1^2 \chi_{ij} \; ; \; p_j = 2\mu l_2^2 \xi_j \; ; \tau_{ijk} = 2\mu l_3^2 \eta_{ijk} \tag{3.18a}$$

$$p_j = 2\mu l_2^2 \xi_j \; ; \tau_{ijk} = 2\mu l_3^2 \eta_{ijk} \tag{3.18b}$$

where λ, μ are Lamé constants; l_1, l_2, l_3 are three material length scale parameters (MLSP) which should be practically determined by experimental works.

3.2.3 Ritz-type series solution

According to the Ritz approach, the following series of approximation functions and associated series values can be used to describe the membrane and transverse displacements $\left(u_1^0, u_2^0, u_3^0, \varphi_1, \varphi_2\right)$ of the microplates:

$$u_1^0(x_1,x_2)=\sum_{i=1}^{n_1}\sum_{j=1}^{n_2}u_{1ij}R_{i,1}\left(x_1\right)P_j\left(x_2\right);\ u_2^0(x_1,x_2)=\sum_{i=1}^{n_1}\sum_{j=1}^{n_2}u_{2ij}R_i\left(x_1\right)P_{j,2}\left(x_2\right)$$

$$u_3^0(x_1,x_2)=\sum_{i=1}^{n_1}\sum_{j=1}^{n_2}u_{3ij}R_i\left(x_1\right)P_j\left(x_2\right);\ \varphi_2(x_1,x_2)=\sum_{i=1}^{n_1}\sum_{j=1}^{n_2}y_{ij}R_i\left(x_1\right)P_{j,2}\left(x_2\right)$$

$$\varphi_1(x_1,x_2)=\sum_{i=1}^{n_1}\sum_{j=1}^{n_2}x_{ij}R_{i,1}\left(x_1\right)P_j\left(x_2\right) \tag{3.36}$$

where $u_{1ij}, u_{2ij}, u_{3ij}, x_{ij}, y_{ij}$ are represent unknown variables need to determined; the shape functions in x_1-, x_2- direction are $R_i\left(x_1\right), P_j\left(x_2\right)$, respectively. As a consequence, only two shape functions affect the five unknowns of the microplates. As mentioned in the introduction section, the accuracy and efficiency of the Ritz method strongly depend on the construction of the approximation functions. In general, these shape functions should be complete, continuous and independently linear. In this study, the Hermite polynomial, Laguerre polynomial and orthogonal polynomials made from Gram Schmidt method which are defined by this recursion formula, are used to develop novel Ritz method's shape functions.

Hermite polynomial:

Hermite polynomial are characterized by the following recursion formula:

$$\begin{cases} He_0(x)=1, \quad He_1(x)=2x, \\ He_n(x)=2xHe_{n-1}(x)-2(n-1)He_{n-2}(x) \end{cases} \tag{3.37}$$

Hermite polynomials satisfy normalization as follows:

$$\int_{-\infty}^{\infty}(He(x))^2e^{-x^2}dx=2^n\sqrt{\pi}n! \tag{3.38}$$

Laguerre polynomial:

Hypergeometric functions define the generalized Laguerre function:

$$\mathrm{L}(n,a,x)=\binom{n+a}{a}{}_1F_1\left(-n;a+1;x\right) \tag{3.39}$$

The function returns orthogonal generalized Laguerre polynomials for nonnegative integer values of n:

$$\left\langle f1, f2\right\rangle=\int_0^{\infty}e^{-x}x^a f_1\left(x\right)f_2\left(x\right)dx \tag{3.40}$$

Furthermore, generalized Laguerre polynomials fulfill this normalization:

$$\left\langle \mathrm{L}(n,a,x),\mathrm{L}(m,a,x)\right\rangle=\begin{cases} 0 & if \quad n\neq m \\ \dfrac{\Gamma\left(a+n+1\right)}{n!} & if \quad n=m \end{cases} \tag{3.41}$$

Gram-Schmidt-based orthogonal polynomials:

Next, the admissible functions known as orthogonal polynomials (OP) which are constructed using the Gram-Schmidt (GS) method. These functions exhibit a rapid convergence rate, although they encounter challenges in determining the initial function. Using the GS approach is defined as follows:

$$\phi_1(x)=(x-A_1)\phi_0(x),\quad \phi_k(x)=(x-A_k)\phi_{k-1}(x)-D_k\phi_{k-2}(x) \tag{3.42a}$$

$$A_k=\frac{\int_c^d xw(x)\phi_{k-1}^2(x)dx}{\int_c^d w(x)\phi_{k-1}^2(x)dx};\ D_k=\frac{\int_c^d xw(x)\phi_{k-1}(x)\phi_{k-2}(x)dx}{\int_c^d w(x)\phi_{k-2}^2(x)dx} \tag{3.42b}$$

where $w(x)$ being the weighting function. The orthogonality is satisfied by the polynomials $\phi_k(x)$ as below:

$$\int_c^d w(x)\phi_k(x)\phi_l(x)=\begin{cases}0 & if \quad k\neq l\\ a_{kl} & if \quad k=l\end{cases} \tag{3.43}$$

with $w(x)=1;\ \phi_0(x)=2x+1$, and $[c,d]\in[-1,1]$.

The combination of clamped and simply-supported BCs on the edges of the microplates leads to the various ones as follows: SSSS, SCSC, CSCS, CCCC which will be taken into account in the numerical examples as follows in the Table 3.1:

Table 3.1: Approximation functions of series solutions with different BCs

Boundary conditions		Approximation functions	
		$R_j(x_1)$	$P_j(x_2)$
SSSS	Ritz-Hermite	$x_1(a-x_1)He_j$	$x_2(b-x_2)He_j$
	Ritz-Laguerre	$x_1(a-x_1)L_j$	$x_2(b-x_2)L_j$
	Ritz-OP	$x_1(a-x_1)\phi_j$	$x_2(b-x_2)\phi_j$
SCSC	Ritz-Hermite	$x_1(a-x_1)^2He_j$	$x_2(b-x_2)^2He_j$
	Ritz-Laguerre	$x_1(a-x_1)^2L_j$	$x_2(b-x_2)^2L_j$
	Ritz-OP	$x_1(a-x_1)^2\phi_j$	$x_2(b-x_2)^2\phi_j$
CSCS	Ritz-Hermite	$x_1^2(a-x_1)\ He_j$	$x_2^2(b-x_2)He_j$
	Ritz-Laguerre	$x_1^2(a-x_1)\ L_j$	$x_2^2(b-x_2)L_j$
	Ritz-OP	$x_1^2(a-x_1)\ \phi_j$	$x_2^2(b-x_2)\phi_j$
CCCC	Ritz-Hermite	$x_1^2(a-x_1)^2He_j$	$x_2^2(b-x_2)^2He_j$
	Ritz-Laguerre	$x_1^2(a-x_1)^2L_j$	$x_2^2(b-x_2)^2L_j$
	Ritz-OP	$x_1^2(a-x_1)^2\phi_j$	$x_2^2(b-x_2)^2\phi_j$

The microplate's characteristic equations of motion:

$$\left(\mathbf{K} - N^0\mathbf{K}^g\right)\mathbf{d} + \mathbf{M}\ddot{\mathbf{d}} = \mathbf{F} \tag{3.44}$$

3.3 Numerical results

3.3.1 Study convergence of solution

The PMF microplates are designed to be made of metal foam materials whose characteristics are followed: $E_{\max} = 200$ GPa, $\rho_{\max} = 7850$ kg/m^3, $\nu_{\max} = 0.33$. For simplicity purpose, the numerical examples utilize the following normalized response parameters $\bar{\omega} = 100\omega h\sqrt{\rho_{\max}/E_{\max}}$. To evaluate the convergence and efficiency of the current computational method, this example will compare the convergence speed and stability of the proposed Hermite-Ritz and Laguerre-Ritz, Exponential-Ritz, OP-Ritz solutions with those of the Ritz solution obtained from other shape functions. The following approximation functions will be used in Eq. (3.36) for the computations:

Static Beam Functions (SBF):

$$F_j\left(x_2\right) = A_j + B_j x_2 + C_j x_2^2 + D_j x_2^3 + \sin\left(jx_2/b\right) \tag{3.47}$$

with $A_j = 0; B_j = -j\pi/b; C_j = j\pi\left(\left(-1\right)^j + 2\right)/b^2; D_j = -j\pi\left(\left(-1\right)^j + 1\right)/b^3$.

Non-Orthogonal Polynomials (NOP):

$$F_j\left(x_2\right) = \left(b - x_2\right)^2 x_2^{j+1} \tag{3.48}$$

Product of Trigonometric Functions (PTF):

$$F_j\left(x_2\right) = \sin\left(\pi x_2/b\right)\sin\left(j\pi x_2/b\right) \tag{3.49}$$

Characteristic Functions (CF):

$$F_j\left(x_2\right) = \sin\alpha_j x_2 - \sinh\alpha_j x_2 - \phi_j\left(\cos\alpha_j x_2 - \cosh\alpha_j x_2\right) \tag{3.50}$$

with $\phi_j = \left(\sin\alpha_j b - \sinh\alpha_j b\right)/\left(\cos\alpha_j b - \cosh\alpha_j b\right); \alpha_j = \left(j + 0.5\right)\pi/b$. It is noted that the functions $T_j\left(x_1\right)$ are defined in a similar way by replacing the variable x_2 for x_1, the length b for the width a in the previous equations. For the purpose of investigating the convergence of approximation functions, the reference distance is defined as follows:

$$d_f = \omega_{i+1} - \omega_i \tag{3.51}$$

where ω_i and ω_{i+1} are results of fundamental frequency of porous metal foam at n_i and n_{i+1}, respectively.

In order to evaluate the convergence of the Ritz solution, Table 3.2 and Fig. 3.6 show the convergence speed of fundamental frequencies of the PMF microplates under fully clamped boundary condition with $a/h = 10$, $\beta = 0.3$ and $h/l = \infty$.

Table 3.2: Comparison with convergence speed of the series solution $\left(n = n_1 = n_2\right)$ of porous metal foam PMF microplates with full clamped boundary condition for

($a/h=10$, $\beta=0.3$, $h/l=\infty$)

Solution	Number of series $n=n_1=n_2$							
	2	3	5	6	8	9	10	15
SBF	11.765	11.27	10.681	10.125	9.905	9.858	9.772	9.4444
NOP	9.455	9.44	9.382	9.373	9.362	9.363	9.362	9.364
PTF	9.784	9.486	9.401	9.400	9.362	9.364	9.362	9.364
CF	9.560	9.545	9.503	9.467	9.402	9.388	9.388	9.388
Hermite	9.649	9.382	9.382	9.382	9.381	9.383	9.384	9.381
Laguerre	9.5341	9.364	9.364	9.364	9.364	9.364	9.364	9.364
OP_GS	9.5571	9.381	9.373	9.373	9.373	9.373	9.373	9.373
Exponential	9.5730	9.406	9.357	9.355	9.355	9.355	9.355	9.355
IGA [174]	9.5202							

Moreover, the line graph compared the convergence speed of seven kinds of shape functions in Fig. 3.6. It is clear that the convergence speeds of the shape functions used to compute the fundamental frequencies are different among shape functions.

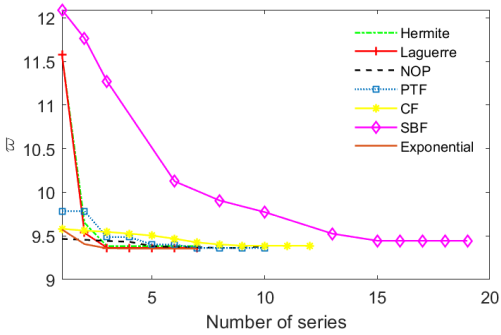

Figure 3.6: Comparison with both convergence speed of number of series of porous metal foam PMF microplates with full clamped boundary condition for normalized fundamental frequency ($a/h=10$, $\beta=0.3$, $h/l=\infty$)

The orthogonal polynomials sequence gave accurate results when computing natural frequencies.

3.3.2 Analysis of PMF microplates

In this example, free vibration $\bar{\omega}=\omega h\sqrt{\rho_{\max}/E_{\max}}$ and buckling loads (uniaxial compression and biaxial compression) $\bar{N}_{cr}=N_{cr}a^2/\left(h^3E_{\max}\right)$ behaviors of the square PMF microplates with simply supported (SSSS) are analysed. The PMF microplates are designed to be made of metal foam materials whose characteristics are followed: $E_{\max}=200$ GPa, $\rho_{\max}=7850$ kg/m^3, $\nu_{\max}=0.33$.

Table 3.3: Normalized fundamental frequencies of PMF rectangular microplates for simply supported boundary condition with $a/h=10$

Type distribution	β	Theory	h/l			
			10	5	2	1
Uniform	0.1	Ritz-Hermite	0.0606	0.0715	0.1234	0.2264
		Ritz-Laguerre	0.0606	0.0715	0.1233	0.2262
	0.2	Ritz-Hermite	0.0592	0.0702	0.1218	0.2240
		Ritz-Laguerre	0.0592	0.0702	0.1218	0.2239
		IGA [20]	0.0601	0.0706	0.1203	0.2196
	0.3	Ritz-Hermite	0.0578	0.0688	0.1201	0.2212
		Ritz-Laguerre	0.0578	0.0688	0.1200	0.2211
		IGA [20]	0.0590	0.0692	0.1179	0.2153

Table 3.4: Normalized critical buckling load under uniaxial compression of PMF rectangular microplates for simply supported boundary condition with $a/h=10$

Type distribution	β	Theory	h/l			
			10	5	2	1
Uniform	0.1	Ritz-Hermite	3.6690	5.0792	14.9412	50.0314
		Ritz-Laguerre	3.6665	5.0754	14.9287	49.9844
		IGA [20]	3.7311	5.1334	14.9043	49.7140
	0.2	Ritz-Hermite	3.3772	4.7119	14.0463	47.2574
		Ritz-Laguerre	3.3748	4.7084	14.0345	47.2129
		IGA [20]	3.4694	4.7734	13.8590	46.2271

3.4 Conclusions

This chapter introduces novel approximation functions for the Ritz method to analyze the behaviors of FG, FG sandwich, FGP, and PMF microplates. A unified higher-order shear deformation theory (HSDT) is formulated to approximate the displacement field accurately. To capture size-dependent effects in microplates, the modified strain gradient theory (MST) is employed. The governing equations of motion are derived using Hamilton's principle. Convergence and validation studies are performed to verify the accuracy and reliability of the proposed solutions.

CHAPTER 4 INTELLIGENT COMPUTATIONAL ALGORITHMS FOR STOCHASTIC ANALYSIS OF FUNCTIONALLY GRADED MICROPLATES WITH UNCERTAINTIES OF MATERIAL PROPERTIES

4.1 Introduction

The main objective of this chapter is to develop a stochastic model for behaviors analysis of the microplates using various advanced algorithms such as Monte Carlo simulation with 10,000 samples, polynomial chaos expansion, stochastic collocation, BCMO-ANN and iBCMO-DNN algorithms.

4.2 Polynomial chaos expansion

In this study, $\hat{u}$ is fundamental frequency or critical buckling load of the FG microplates in terms of a truncated orthogonal series as follows :

$$\hat{u} \approx \hat{u}_{PCE}(\mathbf{x}) = \sum_{i=0}^{P-1} c_i He_i(\mathbf{q}) + r \tag{4.1}$$

where $\hat{u}_{PCE}$ is the response of interest obtained from the PCE; $\mathbf{q}$ is a vector of independent random variables in PCE space mapped to physical random parameters $\mathbf{x}$; He_i are multivariate orthogonal basis functions; c_i are coefficients to be determined so that the residual r is minimized; P is the permutation of the qualified order of the polynomial n

4.3 Stochastic collocation

For 1-D problem (i.e., one random input X) and n_i interpolation points, it approximates the stochastic response u by forming the Lagrange functions and estimating the model response at interpolation points $u(q_i)$ as follows:

$$u(X) \approx \hat{u}(X) = \sum_{i=1}^{n_i} u(q_i) L_i(q) \tag{4.9}$$

where q is a standard variable mapping to the physical variable X and for maximizing performance of this approach q_i are defined as appropriate Gauss quadrature points corresponding to the distribution of q. The 1-D Lagrange interpolation $L_i(q)$ is defined as:

$$L_i(q) = \prod_{\substack{j=1 \\ j \neq i}}^{n_i} (q - q_j) / (q_i - q_j) \tag{4.10}$$

4.4 Intelligent stochastic computational algorithms based on optimization and machine learning methods

4.4.2 Artificial neural network (ANN) and BMCO algorithm: BCMO-ANN

The Artificial Neural Network (ANN) system shown in Fig. 4.2 contains three kinds of layers, namely, input layer, hidden layer, output layer in which each layer consists of neurons that are connected to each other in the previous layer.

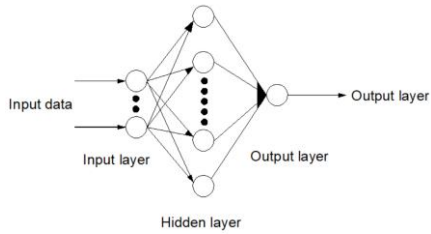

Figure 4.2: An artificial neural network structure

The output data of the activation function for the sum is expressed as follows:

$$y_i^n = \varphi\left(x_i^n\right) = \varphi\left(\sum_{j=1}^{lm_{n-1}} w_{ij}^{n-1} \times y_j^{n-1} + b_i^n\right) \tag{4.24}$$

where y_i^n and x_i^n are data pair output and input of activation function of node i, respectively; w_{ij}^{n-1} is the weight between the output node i and input node j; b_i^n is the bias of node j; φ is the activation function.

4.4.3 Deep neural network (DNN) and improved BMCO algorithm: iBCMO-DNN

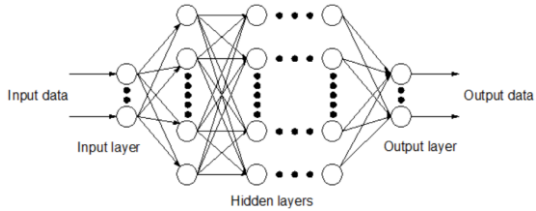

Figure 4.3: Deep neural network

Each node in the succeeding layers will get the total of the preceding nodes' output values multiplied by their respective weights, and the activation function's output data for the sum is supplied as follows:

$$y_i^n = \varphi\left(x_i^n\right) = \varphi\left(\sum_{j=1}^{L_{n-1}} w_{ij}^{n-1} \times y_j^{n-1} + b_i^n\right) \tag{4.26}$$

4.5 Numerical examples

4.5.1 Stochastic vibration analysis of FG microplates using polynomial chaos expansion

In order to investigate of the stochastic responses of the FG microplates, the material properties (E_c, E_m, and ρ_c, ρ_m) are assumed to be randomly distributed via the lognormal distributions and the coefficient of variation (COV) for all random variables is set to equal 10%. The MCS with 10,000 samples is

considered as the exact solutions for comparison purpose. For convenience, the following non-dimensional parameters are used in the numerical examples:

$$\bar{\omega} = \left(\omega a^2 / h\right)\sqrt{\rho_c / E_c} \tag{4.28}$$

Table 4.2: Comparison study between MCS (10.000 samples) and PCE (256 samples) for the mean, standard deviation (SD), Kurtosis and Skewness for the fundamental frequency of the FG microplates ($a/h=10$, MAT 1)

BCs	p	Theory	Mean	SD	Kurtosis	Skewness	COV (%)	Time (s)	Present
$h/l=1$									
SS	1	PCE	11.010	0.5087	2.4628	-0.0532	4.6	17.02	11.010
SS		MCS	11.010	0.5087	2.4633	-0.0531	4.6	814.1	
	5	PCE	8.7431	0.8313	2.6301	0.1966	9.5	18.1	8.720
		MCS	8.7456	0.8317	2.6308	0.1962	9.5	815.3	
	10	PCE	8.0719	0.8990	2.6953	0.2624	11.1	18.4	8.044
		MCS	8.0747	0.8986	2.6949	0.2629	11.1	817.0	
	…								

It can be observed that all statistical moments obtained from MCS and PCE show good agreement in all cases. The required computational time of the present approach is about 1/47 compared with direct MCS method.

Table 4.2 compares the standard deviation (SD), mean, kurtosis and skewness, which are the first four statistical moments of the natural frequencies as calculated by the SC and MCS models for a range of p and a/h values.

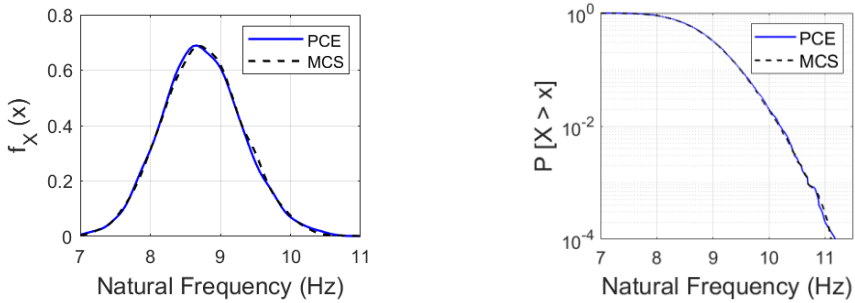

Figure 4.6a: PDF and PoE of MCS and PCE methods for the fundamental frequency (Hz) of the FG microplates with SSSS BC ($p=5$, $h/l=1$, $a/h=10$)

Figs. 4.6a compare the probability density function (PDF) and probability of exceedance (PoE) of MCS and PCE for the vibration analysis of the microplates with various SSSS BC. It can be observed again that the results of MCS are in

good agreement with PCE. It is consistent with what is observed from the comparison of the COV of these stochastic responses shown in Fig. 4.8.

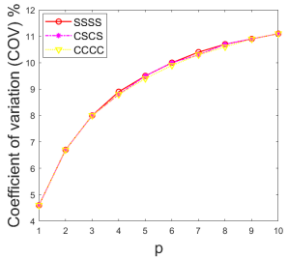

Fundamental frequencies , $h/l=1$

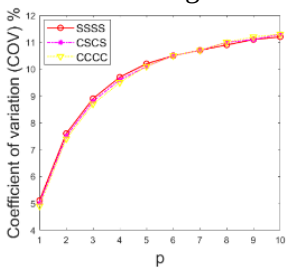

Fundamental frequencies , $h/l=5$

Figure 4.8: Coefficient of variation (COV) with respect the power-law index p of the FG microplates ($a/h=10$) with various BCs and

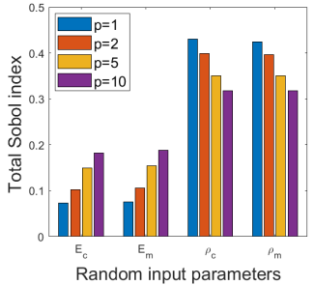

Fundamental frequency, $h/l=1$

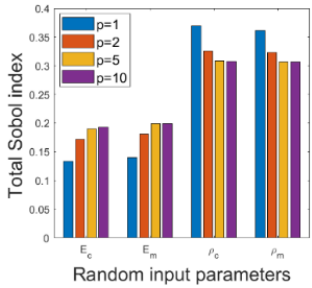

Fundamental frequency, $h/l=5$

Figure 4.11: Total Sobol index of the random input variables with respect to the fundamental frequencies and critical buckling loads of the CCCC FG microplates ($a/h=10$)

Fig 4.11 compares the sensitivity indices based on the total Sobol indices for the vibration analysis using MCS and PCE.

4.5.2 Stochastic thermal buckling analysis of FG sandwich microplates using stochastic collocation

For the SC model with the Gauss quadrature point, only 256 samples are needed. Table 4.3 list the results of the FG sandwich microplates with $h/l=1$ and $h/l=5$ for two types of BCs, a/h and p. The statistical moments derived from SC and MCS exhibit strong concordance. It is noted that this case's computing time is around 1/10 of the time required by the direct MCS technique. Again, for both SC and MCS, the mean values of the critical buckling temperature are quite similar to the corresponding deterministic responses.

Table 4.1: The standard deviation (SD), mean, Skewness, Kurtosis for the biaxial thermal buckling of FG sandwich microplates (MAT 3, $a/h=10$) under linear distribution of SC (256 samples) and MCS (10.000 samples), $T_b = 25^oC$

BCs	p	Theory	Mean	SD	Kurtosis	Skewness	COV (%)	Time (s)	Present
1-1-1									
$h/l=1$									
SS	0.5	SC	10.023	0.8972	3.7410	0.5955	8.9	30	9.9421
SS		MCS	10.017	0.8962	3.7306	0.5927	8.9	325	
	2	SC	9.8862	0.8221	3.4865	0.5257	8.3	33	9.8221
		MCS	9.9028	0.8225	3.4923	0.5270	8.3	330	
CC	0.5	SC	37.498	3.3337	3.4160	0.5005	9.0	40	37.1999
CC		MCS	37.498	3.3363	3.4145	0.4994	9.0	342	
	2	SC	37.460	3.1073	3.4426	0.4919	8.3	41	37.2542
		MCS	37.452	3.1061	3.4461	0.4912	8.3	340	

4.5.3 Stochastic vibration analysis of FGP microplates using BCMO-ANN algorithm

In order to investigate stochastic behaviors of FGP microplates, four random variables of material properties ($E_{m,i}, E_{c,i}, p_{m,i}, p_{c,i}$) are employed with the population size $NP=500$. It is noted that the weight and bias values are automatically updated according to Levenberg - Marquardt optimization, the number of nodes in each hidden layer is 21.

Table 4.4: Mean and standard deviation (SD) of normalized fundamental frequencies for FG microplates with $a/h=10$ and SSSS boundary condition

β	p	h/l	Theory	Mean	SD	Time(s)	Present
0.1	1	10	Ritz-BCMO	4.4049	0.0496	615	4.4073
			BCMO-ANN	4.4090	0.0491	10	
		5	Ritz-BCMO	4.7449	0.0517	620	4.7485
			BCMO-ANN	4.7451	0.0513	9	
		1	Ritz-BCMO	11.0692	0.1051	617	11.0673
			BCMO-ANN	11.0745	0.1059	11	
	10	10	Ritz-BCMO	3.3994	0.0953	625	3.4012
			BCMO-ANN	3.4040	0.0961	10	
		5	Ritz-BCMO	3.5922	0.0997	623	3.6001
			BCMO-ANN	3.6037	0.0993	12	
		1	Ritz-BCMO	7.5662	0.1991	627	7.5531
			BCMO-ANN	7.5376	0.1983	10	
		….					

The dataset, which consists of input-output pairs and training samples are randomly generated through iterations in the ANN training process. In addition, in the prediction process, training samples in the dataset are divided into two groups, in which 80% pairs in data is used for the training set and 20% for the test set. Tables 4.4 presents the mean and standard deviation (SD) of normalized fundamental frequencies of Al/Al_2O_3 FGP microplates with different boundary conditions for both Ritz–BCMO and BCMO-ANN models.

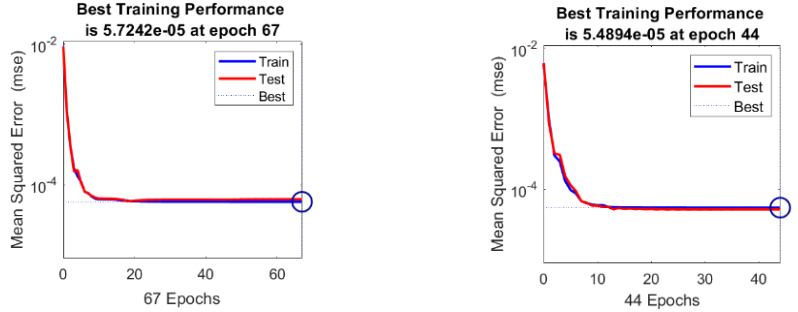

(a) SSSS, $\beta = 0.1$ (b) SSSS, $\beta = 0.2$

Figure 4.19: Loss function of the normalized fundamental frequencies for FGP microplates with different boundary conditions, $p = 10$, $a/h = 10$ and $h/l = 5$

4.5.4 Stochastic thermal buckling analysis of FGP microplates using iBCMO-DNN algorithm

In order to investigate stochastic critical buckling temperatures of FGP microplates, it is noted that five random variables of material properties $\left(E_{m,i}, E_{c,i}, \alpha_{t,i}, \alpha_{m,i}, \rho\right)$ are designed to be randomly distributed with the same population size $NP = 2000$. Additionally, the data training was generated from the earlier analysis of Ritz-iBCMO solution.

For Al/Al_2O_3 FGP microplates with three boundary conditions, the mean and standard deviation of normalized critical buckling temperatures from the Ritz-iBCMO and iBCMO-DNN models are shown in Tables 4.9. The critical buckling temperature responses are computed for the side-to-thickness ratio $a/h = 20$, porous parameter $\beta = 0.1$ and 0.3, power-law index $p = 0.5$ and 2, length scale parameter $h/l = 1$ and 10. Obviously, the statistical moments of the critical buckling temperatures derived from the Ritz-iBCMO and iBCMO-DNN show good agreements for all cases.

Table 4.9: Mean and standard deviation (SD) of normalized critical buckling temperature for FGP microplates with biaxial compression, $a/h=20$, SSSS under uniform temperature distribution

β	p	h/l	Theory	Mean	SD	Time(s)	Present
0.1	0.5	10	Ritz-iBCMO	0.3291	0.0089	2123	0.3284
			iBCMO-DNN	0.3307	0.0091	845	
		1	Ritz-iBCMO	5.1633	0.1343	2125	5.1596
			iBCMO-DNN	5.1688	0.1347	844	
	2	10	Ritz-iBCMO	0.2239	0.0066	2124	0.2236
			iBCMO-DNN	0.2259	0.0071	845	
		1	Ritz-iBCMO	3.8358	0.1084	2123	3.8278
			iBCMO-DNN	3.8315	0.1082	846	

…

Additionally, the performance of the current iBCMO-DNN algorithm in predicting buckling temperature responses is also shown in Figs. 4.24 abc.

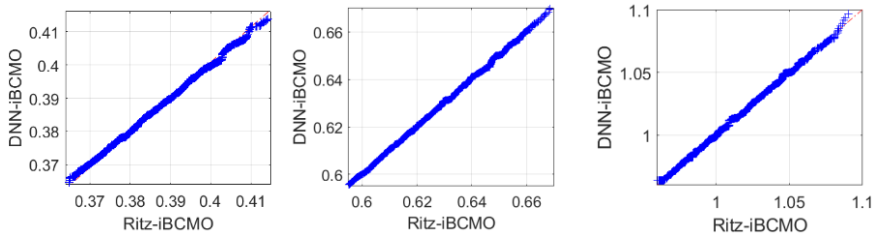

(a) SSSS, $\beta=0.1$ (b) SCSC, $\beta=0.1$ (c) CCCC, $\beta=0.1$

Figure 4.24: Quantile-quantile plot of the Ritz-iBCMO model with DNN-iBCMO, $a/h=20$, $p=1$, $h/l=5$, biaxial compression under uniform distribution

4.6. Conclusions

In order to investigate the stochastic responses of microplates under uncertainty in material properties, the Polynomial Chaos Expansion (PCE), Stochastic Collocation (SC) method, and Monte Carlo method are employed. Moreover, this research proposed a novel intelligent computational algorithm, iBCMO-DNN, for stochastic buckling temperature analysis of microplates with uncertainty of material properties. A combination of BCMO-ANN has been proposed to predict stochastic vibration behaviors of microplates subjected to uncertainties of material properties. The DNN with the long short-term memory model has been employed as a surrogate method to replace the time-consuming computational model, while the iBCMO for searching the set of optimal solutions.

CHAPPTER 5 META-HEURISTIC OPTIMIZATION ALGORITHMS FOR VIBRATION AND BUCKLING OPTIMIZATION OF LAMINATED COMPOSITE PLATES

5.1. Introduction

A brief literature survey indicates that the BCMO and SGA algorithms are recognized as efficient methods for optimization of structures. However, there is no identified research employing these algorithms specifically for solving optimization problems related to laminated composite plates. This study aims to address existing gaps by proposing meta-heuristic optimization algorithms to determine the critical buckling loads and fundamental frequencies of laminated composite plates.

5.2. Theoretical formulation

The unified HSDT for laminated composite plates:

$$\begin{aligned} u_1(x_1,x_2,x_3,t) &= \phi_1(x_1,x_2)\Psi_2(x_3)+u_{3,1}^0\Psi_1(x_3)+u_1^0(x_1,x_2)\\ u_2(x_1,x_2,x_3,t) &= \phi_2(x_1,x_2)\Psi_2(x_3)+u_{3,2}^0\Psi_1(x_3)+u_2^0(x_1,x_2)\\ u_3(x_1,x_2,x_3,t) &= u_3^0(x_1,x_2) \end{aligned} \tag{5.1}$$

where $\Psi_2(x_3)=H^s\Phi(x_3), \Psi_1(x_3)=H^s\Phi(x_3)-x_3$;. The relationship between the strains and stresses for the k layer is expressed as:

$$\boldsymbol{\sigma}=\begin{Bmatrix}\sigma_{11}\\ \sigma_{22}\\ \sigma_{12}\\ \sigma_{13}\\ \sigma_{23}\end{Bmatrix}=\begin{bmatrix}\bar{Q}_{11}^{(k)} & \bar{Q}_{12}^{(k)} & \bar{Q}_{16}^{(k)} & 0 & 0\\ \bar{Q}_{12}^{(k)} & \bar{Q}_{22}^{(k)} & \bar{Q}_{26}^{(k)} & 0 & 0\\ \bar{Q}_{16}^{(k)} & \bar{Q}_{22}^{(k)} & \bar{Q}_{66}^{(k)} & 0 & 0\\ 0 & 0 & 0 & \bar{Q}_{55}^{(k)} & \bar{Q}_{45}^{(k)}\\ 0 & 0 & 0 & \bar{Q}_{45}^{(k)} & \bar{Q}_{44}^{(k)}\end{bmatrix}\begin{Bmatrix}\varepsilon_{11}\\ \varepsilon_{22}\\ \gamma_{12}\\ \gamma_{13}\\ \gamma_{23}\end{Bmatrix}=\bar{\mathbf{Q}}_{\varepsilon}\boldsymbol{\varepsilon} \tag{5.4}$$

where

$$\bar{Q}_{11}^{(k)}=Q_{22}^{(k)}\sin^4\alpha+Q_{11}^{(k)}\cos^4\alpha+2\left(2Q_{66}^{(k)}+Q_{12}^{(k)}\right)\cos^2\alpha\sin^2\alpha \tag{5.5a}$$

$$\bar{Q}_{12}^{(k)}=Q_{12}^{(k)}\left(\cos^4\alpha+\sin^4\alpha\right)+\left(Q_{11}^{(k)}-4Q_{66}^{(k)}+Q_{22}^{(k)}\right)\cos^2\alpha\sin^2\alpha \tag{5.5b}$$

$$\bar{Q}_{22}^{(k)}=2\left(2Q_{66}^{(k)}+Q_{12}^{(k)}\right)\cos^2\alpha\sin^2\alpha+Q_{11}^{(k)}\sin^4\alpha+Q_{22}^{(k)}\cos^4\alpha \tag{5.5c}$$

$$\bar{Q}_{16}^{(k)}=\left(2Q_{66}^{(k)}+Q_{12}^{(k)}-Q_{22}^{(k)}\right)\sin^3\alpha\cos\alpha+\left(Q_{11}^{(k)}-\left(Q_{12}^{(k)}+2Q_{66}^{(k)}\right)\right)\sin\alpha\cos^3\alpha \tag{5.5d}$$

$$\bar{Q}_{26}^{(k)}=\left(2Q_{66}^{(k)}+Q_{12}^{(k)}-Q_{22}^{(k)}\right)\sin\alpha\cos^3\alpha+\left(Q_{11}^{(k)}-\left(Q_{12}^{(k)}+2Q_{66}^{(k)}\right)\right)\sin^3\alpha\cos\alpha \tag{5.5e}$$

$$\bar{Q}_{66}^{(k)} = \left(Q_{22}^{(k)} + Q_{11}^{(k)} - 2\left(Q_{12}^{(k)} + Q_{66}^{(k)}\right)\right)\cos^2\alpha\sin^2\alpha + Q_{66}^{(k)}\left(\cos^4\alpha + \sin^4\alpha\right) \quad (5.5f)$$

$$\bar{Q}_{44}^{(k)} = Q_{44}^{(k)}\cos^2\alpha + Q_{55}^{(k)}\sin^2\alpha\,;\ \bar{Q}_{55}^{(k)} = Q_{44}^{(k)}\sin^2\alpha + Q_{55}^{(k)}\cos^2\alpha \quad (5.5g)$$

$$\bar{Q}_{45}^{(k)} = \left(Q_{55}^{(k)} - Q_{44}^{(k)}\right)\cos\alpha\sin\alpha \quad (5.5k)$$

with α is the fiber angle in each layer, $Q_{ij}^{(k)}$ of the orthotropic composite plates in the local coordinate system are given by:

$$Q_{11}^{(k)} = \frac{E_1}{1-\nu_{12}\nu_{21}}, Q_{12}^{(k)} = \frac{\nu_{12}E_2}{1-\nu_{12}\nu_{21}}, Q_{22}^{(k)} = \frac{E_2}{1-\nu_{12}\nu_{21}}, \qquad Q_{66}^{(k)} = G_{12}, Q_{44}^{(k)} = G_{23}, Q_{55}^{(k)} = G_{13} \quad (5.6b)$$

5.3. Ritz method

The membrane and transverse displacements, as well as rotations $\left(u_1^0, u_2^0, u_3^0, \phi_1, \phi_2\right)$ can be represented through a series of shape functions in x_1-, x_2- direction ($X_i\left(x_1\right)$ and $Y_j\left(x_2\right)$) and five unknowns variables ($u_{1ij}, u_{2ij}, u_{3ij}, x_{ij}, y_{ij}$), expressed as follows:

$$u_2^0(x_1,x_2,t) = \sum_{i=1}^{n_1}\sum_{j=1}^{n_2} u_{2ij}(t)Y_{j,2}(x_2)X_i(x_1) \quad (5.15a)$$

$$u_1^0(x_1,x_2,t) = \sum_{i=1}^{n_1}\sum_{j=1}^{n_2} u_{1ij}(t)Y_j(x_2)X_{i,1}(x_1) \quad (5.15b)$$

$$\phi_2(x_1,x_2,t) = \sum_{i=1}^{n_1}\sum_{j=1}^{n_2} y_{ij}(t)Y_{j,2}(x_2)X_i(x_1) \quad (5.15c)$$

$$\phi_1(x_1,x_2,t) = \sum_{i=1}^{n_1}\sum_{j=1}^{n_2} x_{ij}(t)Y_j(x_2)X_{i,1}(x_1) \quad (5.15d)$$

$$u_3^0(x_1,x_2,t) = \sum_{i=1}^{n_1}\sum_{j=1}^{n_2} u_{3ij}(t)Y_j(x_2)X_i(x_1) \quad (5.15e)$$

5.4. Optimization algorithm

In this section, three algorithms are presented to identify the fiber angle α that maximize the critical buckling loads and frequencies of laminated composite plates, with the following objective functions.

Maximum $\bar{\omega} = f\left(\alpha_i^d\right)$ or $\bar{N}_{cr} = f\left(\alpha_i^d\right)$

$$\text{Subjected to } -90^o \le \alpha_i^d \le 90^o \quad (5.23)$$

with d is the number of layers.

Three algorithms including differential evolution (DE), shrimp and goby association search algorithm (SGA) and balancing composite motion optimization (BCMO) are used to solve the above optimization problem.

5.5. Numerical examples

5.5.2. Optimization study

In order to compare the efficacy of various meta-heuristics, Figs. 5.4 shows the convergence histories of natural frequencies and buckling loads of SSSS plates by three different solutions (DE, SGA, and BCMO). It can be seen that the SGA and BCMO algorithms converge faster than the DE one.

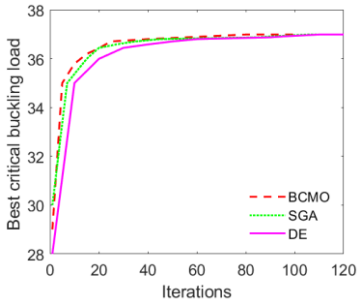

a) Symmetric layers

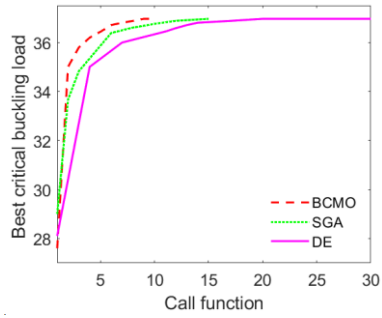

b) Arbitrary layers

Figure 5.4: Comparison the maximum buckling load (uniaxial compression) of SSSS square laminated composite plates with size population $NP = 20$ ($E_1 / E_2 = 40$)

5.6. Conclusions

This chapter studies meta-heuristic optimization algorithms for vibration and buckling analysis of laminated composite plates. The theoretical framework incorporates a unified HSDT, Ritz method, BCMO, and SGA. The obtained numerical results showed an efficiency and accuracy of the present theory in predicting the responses of laminated composite plates.

CHAPPTER 6 CONCLUSIONS AND RECOMMENDATIONS

6.1 Conclusions

The dissertation has developed new approximation functions for the Ritz method; developed stochastic models for analysis behaviors of FG, FG sandwich, FGP, PMF plates and microplates; developed two novel intelligent computation algorithms for solving the stochastic problems of microplates; proposed two optimization methods to search the optimal fiber directions of laminated composite plates. The unified higher-order shear deformation theory (HSDT) theory has been formulated to approximate of the displacement field. The modified gradient strain theory (MST) and the modified couple stress theory (MCT) are employed in the analysis of microplates, taking into account their

size-dependent behavior. The governing equations of motion are obtained using Hamilton's principle. Convergence and verification studies are conducted to establish the precision of the proposed solution. This study presents numerical results investigating the influence of material distribution, material length scale parameters, porosity density, temperature variations, and boundary conditions on the natural frequencies, critical buckling loads, and deflections of functionally graded microplates.

While the current shape functions have demonstrated effectiveness on two-dimensional microplates, their application on three-dimensional plates and microplates poses certain challenges. Furthermore, the present thesis fails to account for the behavioral characteristics of laminated composite microplates in situations where the fiber direction undergoes uncertain variations. The current methodology encounters challenges when dealing with plates that have arbitrary boundary conditions. Additionally, the thesis currently does not address the issue of microplates with periodic boundary conditions.

6.2. Recommendations

The following are some suggestions for how to proceed with the projected expansion of the study in the future:

- The novel shape functions can be developed to analysis behaviors of laminated composite microplates for two-dimensional and three-dimensional.
- Analysis of skew composite/FG microplates can be developed by extending present methods.
- A nonlinear model based on large displacements, rotations, and the Ritz method should be considered for the analysis of composite and FGP microplates under the arbitrary boundary conditions.
- Address the issue of microplates with periodic boundary conditions.